Plant hydraulics accentuates the effect of atmospheric moisture stress on transpiration

Yanlan Liu [1✉], Mukesh Kumar[2], Gabriel G. Katul[3], Xue Feng[4] and Alexandra G. Konings[1]

[1]Department of Earth System Science, Stanford University, Stanford, CA, USA. [2]Department of Civil, Construction, and Environmental Engineering, University of Alabama, Tuscaloosa, AL, USA. [3]Nicholas School of the Environment, Duke University, Durham, NC, USA. [4]Department of Civil, Environmental and Geo-Engineering, University of Minnesota, Twin Cities, MN, USA. ✉e-mail: yanlan@stanford.edu

Plant hydraulics accentuates the effect of atmospheric moisture stress on transpiration

Yanlan Liu[1][*], Mukesh Kumar[2], Gabriel G. Katul[3],
Xue Feng[4], Alexandra G. Konings[1]

[1]Department of Earth System Science, Stanford University, Stanford, CA 94305, USA

[2]Department of Civil, Construction, and Environmental Engineering, University of Alabama, Tuscaloosa, AL 35401, USA

[3]Nicholas School of the Environment, Duke University, Durham, NC 27708, USA

[4]Department of Civil, Environmental and Geo-Engineering, University of Minnesota, Twin Cities, MN 55455, USA

[*]To whom correspondence should be addressed; E-mail: yanlan@stanford.edu

List of contents

- Supplementary Notes 1–3

- Supplementary Table 1

- Supplementary Figures 1–3

Supplementary Notes

(1) Calculation of evaporation and transpiration

Evaporation from the ground surface (E_g) and transpiration through the leaves (E_l) are calculated based on the Penman-Monteith equation derived from energy balance. The total net radiation (R_n) is partitioned into the fraction absorbed by leaves (R_{nl}) and the fraction that penetrates through the canopy to the ground surface (R_{ng}) following Beer's law.

$$R_n = R_{ng} + R_{nl} \tag{16}$$

$$R_{ng} = R_n \exp\left(-k\,\text{LAI}\right) \tag{17}$$

$$R_{ng} = H_g + \lambda E_g \tag{18}$$

$$R_{nl} = H_l + \lambda E_l \tag{19}$$

where k is the canopy extinction coefficient calculated using solar zenith angle assuming a spherical leaf angle distribution [1]; LAI is the leaf area index; H_g and H_l are the sensible heat flux on the ground and canopy surfaces respectively; λ is the latent heat of vaporization.

On the ground and canopy surfaces,

$$H_g = g_g^h\,C_p\,(T_g - T_a) \tag{20}$$

$$E_g = g_g^v\,[e_s(T_g) - e(T_a)]\,/P_0 \tag{21}$$

$$H_l = g_l^h\,C_p\,(T_l - T_a) \tag{22}$$

$$E_l = g_l^v\,[e_s(T_l) - e(T_a)]\,/P_0 \tag{23}$$

where C_p is the specific heat capacity of air; T_g, T_l and T_a are the temperatures on the ground surface, canopy surface, and in the air respectively; e_s and e are the saturated and actual vapor pressure corresponding to given temperature respectively; P_0 is the atmospheric pressure; g_g^h, g_g^v, g_l^h and g_l^v are the conductances for heat (superscript h) or water vapor (superscript v) from the ground surface (subscript g) or the canopy surface (subscript l) to the atmosphere above the canopy (height of eddy covariance measurement). The conductances are calculated based on

resistances in series.

$$g_g^h = \left[g_a'^{-1} + g_a^{-1} \right]^{-1} \tag{24}$$

$$g_g^v = \left[g_g^{h^{-1}} + g_{soil}^{-1} \right]^{-1} \tag{25}$$

$$g_l^h = g_a \tag{26}$$

$$g_l^v = \left[g_a^{-1} + (g_s \, \text{LAI})^{-1} \right]^{-1} \tag{27}$$

where g_a' and g_a are the aerodynamic conductances below and above the canopy, calculated as functions of wind speed, friction velocity, canopy height, and measurement height following [1, 2]. A stability correction on g_a is incorporated as described in [1]. The g_{soil} is the soil surface obtained based on the top layer soil moisture, following [2]. g_s is the stomatal conductance at a leaf level calculated using either an empirical or a hydraulic representation as described in Methods.

Combining Eq. 18–23, evaporation and transpiration can be solved using the Penman-Monteith equations:

$$E_g = \frac{\Delta R_{ng} + P_0 \, C_p \, g_g^h \, D}{\Delta \lambda + P_0 \, C_p \, g_g^h / g_g^v} \tag{28}$$

$$E_l = \frac{\Delta R_{nl} + P_0 \, C_p \, g_l^h \, D}{\Delta \lambda + P_0 \, C_p \, g_l^h / g_l^v} \tag{29}$$

where Δ is the rate of change of saturated vapor pressure with air temperature; and D is the vapor pressure deficit.

(2) Physiological constraints imposed in MCMC

Two physiological constraints based on previous meta-analyses were incorporated in the MCMC optimization process. Samples that did not satisfy the two constraints were discarded. The first constraint is that leaf water potential corresponding to stomatal closure is generally higher than -4 MPa across species ($\psi_{\text{close}} \geq -4$ MPa) [3]. The second constraint is that leaf water potential corresponding to 50% loss of stomatal conductance is generally higher than that corresponding to 50% of xylem conductance ($\psi_{gs,50} > \psi_{50}$) [4]. That is, stomatal closure occurs earlier than xylem embolism [5].

To implement the first constraint, according to Eq. 9 (Methods), the marginal water use efficiency (λ_{close}) corresponding to stomatal closure ($g_s = 0$) is $c_a/(a_0 D)$. Combining with Eq. 6 (Methods), the leaf water potential corresponding to stomatal closure is

$$\psi_{\text{close}} = \frac{1}{\beta_0} \ln \left(\frac{c_a}{a_0 D \lambda_W} \right) \tag{30}$$

where c_a and a_0 are constants (see Methods) and the average of day-time VPD is used as D for each site. Setting Eq. 30 greater than -4 MPa imposes a physiologically feasible constraint on the combination of β_0 and λ_W. The probability distribution of ψ_{close} across sites calculated using site-specific VPD and posterior samples of λ_W and β_0 under constraint is shown in Supplementary Fig. 1a.

To implement the second constraint, according to Eq. 9 (Methods), the stomatal conductance at half closure is

$$g_{s,50} = \alpha \left[-1 + \left(\frac{c_a}{a_0 \lambda(\psi_{gs,50})} \right)^{1/2} D^{-1/2} \right] = \frac{1}{2} \alpha \left[-1 + \left(\frac{c_a}{a_0 \lambda_W} \right)^{1/2} D^{-1/2} \right] \tag{31}$$

Combining with Eq. 6 (Methods), $\psi_{gs,50}$ can be obtained as

$$\psi_{gs,50} = -\frac{2}{\beta_0} \ln \left(\frac{1}{2} \sqrt{\frac{a_0 D \lambda_W}{c_a}} + \frac{1}{2} \right) \tag{32}$$

Setting Eq. 32 greater than ψ_{50} poses a physiological constraint on possible combinations of ψ_{50}, β_0 and λ_W. Estimated $\psi_{gs,50}$ across sites using posterior samples are compared with ψ_{50} in Supplementary Fig. 1b.

Overall, the majority of posterior samples of the hydraulic traits lead to ψ_{close} and $g_{s,50}$ away from the two constraints (Supplementary Fig. 1, red lines). This indicates the robustness of the inferred hydraulic traits with respect to the exact constraining thresholds (i.e., the -4 MPa threshold for ψ_{close} and the 1:1 slope between $\psi_{gs,50}$ and ψ_{50}), which might vary with available data in the meta-analysis [3, 4]. In addition, the retrieved pattern of $\psi_{gs,50}$ and ψ_{50} (Supplementary Fig. 1b) is also consistent with a global comparison between these two traits [6], indicating a wide range of ψ_{50} from -10 MPa to 0 MPa in contrast to $\psi_{gs,50}$ mostly being above -2 MPa and ψ_{50}.

(3) Attribution analysis on the restriction effect of VPD on ET in the hydraulic model

This section analyzes the contributions of three factors that contribute to the relatively high restriction effect of VPD on ET in the hydraulic model (Fig. 3, main text). The three factors that are distinct from those of the empirical model include: (1) the overall higher magnitude of g_s^* and m due to the hydraulic constraint (difference in mean); (2) the dynamics of m as a function of leaf water potential as opposed to a constant value in the empirical model; and (3) the different dynamical pattern of g_s^* with leaf water potential in contrast to varying with soil moisture. To evalute the impact of difference in the mean of g_s^* and m, a modified version of Eq. 11 (Methods) as below is used.

$$g_{s,1} = g_{s,Hydr}^* \frac{\overline{g_{s,Empr}^*}}{\overline{g_{s,Hydr}^*}} \left(1 - m_{Hydr} \frac{\overline{m_{Empr}}}{\overline{m_{Hydr}}} \ln D\right) \tag{33}$$

where $\overline{g_{s,Empr}^*}$ and $\overline{g_{s,Hydr}^*}$ are the temporal averages of reference stomatal conductance estimated using the empirical and hydraulic model, respectively; $\overline{m_{Empr}}$ and $\overline{m_{Hydr}}$ are the temporal averages of the VPD-sensitivity estimated using the empirical and the hydraulic model, respectively. The $g_{s,Hydr}^*$ and m_{Hydr} were calculated numerically using the full stomatal model (Eq. 5 in Methods) as $g_{s,Hydr}^* = g_{s,Hydr}(D = 1\text{kPa})$ and $m_{Hydr} = (1 - g_{s,Hydr}/g_{s,Hydr}^*)/\ln D$, respectively. Eq. 33 forces the temporal average of the VPD-sensitivity in the hydraulic model being equal to that in the empirical model, and correspondingly correct the difference in the mean value of the reference stomatal conductance. Thus $g_{s,1}$ yields an ET without the difference in the mean of VPD-sensitivity between the two models. The contribution of difference in the mean of g_s^* and m to the restriction effect of VPD on ET can then be quantified as the difference between the restriction effect calculated using the original hydraulic model and that using $g_{s,1}$. For mathematical tractability, a reference VPD of $D_0 = 1$ kPa is used to calculate the restriction effect (Eq. 15, Methods) in this section.

Likewise, to evaluate the impact of the dynamics of the VPD-sensitivity, m_{Hydr} in Eq. 11 (Methods) is artificially held constant as its temporal average $\overline{m_{Hydr}}$, i.e.,

$$g_{s,2} = g_{s,Hydr}^* \left(1 - \overline{m_{Hydr}} \ln D\right) \tag{34}$$

Thus $g_{s,2}$ leads to an ET without dynamics in VPD-sensitivity and the contribution of this dy-

namics can be quantified as the difference between the restriction effect calculated using the original hydraulic model and that using $g_{s,2}$.

To evaluate the impact of the dynamics of the reference stomatal conductance, $g^*_{s,Hydr}$ in Eq. 11 (Methods) is artificially changed into $g^*_{s,Empr}$ while correcting the mean to ensure the temporal mean remains unchanged, i.e.,

$$g_{s,3} = g^*_{s,Empr} \frac{\overline{g^*_{s,Hydr}}}{\overline{g^*_{s,Empr}}} \left(1 - \overline{m_{Hydr}} \ln D\right) \tag{35}$$

Thus $g_{s,3}$ leads to an ET with the dynamical pattern of the reference stomatal conductance the same as that in the empirical model. The impact of the different dynamics of $g_{s,Hydr}$ with respect to $g_{s,Empr}$ can then be quantified as the difference between the restriction effect calculated using the original hydraulic model and that using $g_{s,3}$.

Supplementary Table

Table 1: Location, plant functional type (PFT), canopy height (Z_c), maximum rooting depth (Z_r), and soil texture of the studied FLUXNET sites. PFTs of the sites include evergreen broadleaf forests (EBF), mixed forests (MF), evergreen needleleaf forests (ENF), croplands (CRO), and grasslands (GRA).

Site ID	Latitude	Longitude	PFT	Z_c (m)	Z_r (m)	Soil texture	Reference
AU-Wac	-37.43	145.19	EBF	80	9.0	sandy loam	[7]
AU-Wom	-37.42	144.09	EBF	25	3.5	sandy loam	–
BE-Lon	50.55	4.75	CRO	1	0.1	loam	[8]
BE-Vie	50.31	6.00	MF	28	1.1	silt loam	[9]
BR-Sa3	-3.02	-54.97	EBF	37	8.3	loam	–
CA-NS1	55.88	-98.48	ENF	20	0.2	loam	–
CA-NS2	55.91	-98.52	ENF	20	0.2	loam	–
CA-NS3	55.91	-98.38	ENF	7	0.2	loam	–
CA-SF1	54.49	-105.82	ENF	6	2.1	sandy loam	[10]
CH-Oe2	47.29	7.73	CRO	1	0.1	sandy clay	[11]
CN-Cha	42.40	128.10	MF	28	0.2	silt loam	[12]
CN-Din	23.17	112.54	EBF	31	1.2	loam	–
CN-Qia	26.74	115.06	ENF	23	4.6	loam	–
DE-Geb	51.10	10.91	CRO	1	0.4	loamy sand	[13]
DE-Hai	51.08	10.45	DBF	33	0.5	silt clay	[14]
DE-Kli	50.89	13.52	CRO	1	0.2	clay loam	[15]
DE-Lkb	49.10	13.30	ENF	18	1.0	loam	[16]
DE-Obe	50.79	13.72	ENF	25	2.3	loam	–
DE-Seh	50.87	6.45	CRO	1	0.3	loam	[17]
DK-Sor	55.49	11.64	DBF	26	1.1	loam	[18]
FI-Hyy	61.85	24.29	ENF	18	1.2	sandy loam	[19]
FR-Gri	48.84	1.95	CRO	1	0.6	silt loam	[20]
FR-LBr	44.72	-0.77	ENF	18	0.8	sandy loam	[21]
IT-CA3	42.38	12.02	DBF	3	1	loam	[22]
IT-Col	41.85	13.59	DBF	20	2.5	loam	[23]
IT-Isp	45.81	8.63	DBF	23	0.5	sandy loam	[24]
IT-Lav	45.96	11.28	ENF	33	1.8	loam	[25]
IT-MBo	46.01	11.05	GRA	0.3	0.1	loam	[26]
IT-PT1	45.20	9.06	DBF	26	0.2	sandy loam	[27]
IT-Ren	46.59	11.43	ENF	27	2.5	loam	[28]
IT-Ro1	42.41	11.93	DBF	15	0.5	sandy clay	[29]
NL-Hor	52.24	5.07	GRA	0.3	0.1	loam	[30]
RU-Fyo	56.46	32.92	ENF	27	1.5	sandy loam	[31]
US-Blo	38.90	-120.63	ENF	8	2.0	sandy clay loam	[32]
US-Me2	44.45	-121.56	ENF	33	2.0	sandy loam	[33]
US-MMS	39.32	-86.41	DBF	27	2.2	silt loam	[34]
US-NR1	40.03	-105.55	ENF	12	0.6	loamy sand	[35]
US-Prr	65.12	-147.49	ENF	11	0.2	loamy sand	–
US-UMB	45.56	-84.71	DBF	20	2.0	sand	[36]
US-UMd	45.56	-84.70	DBF	22	0.4	sand	[37]

Supplementary Figures

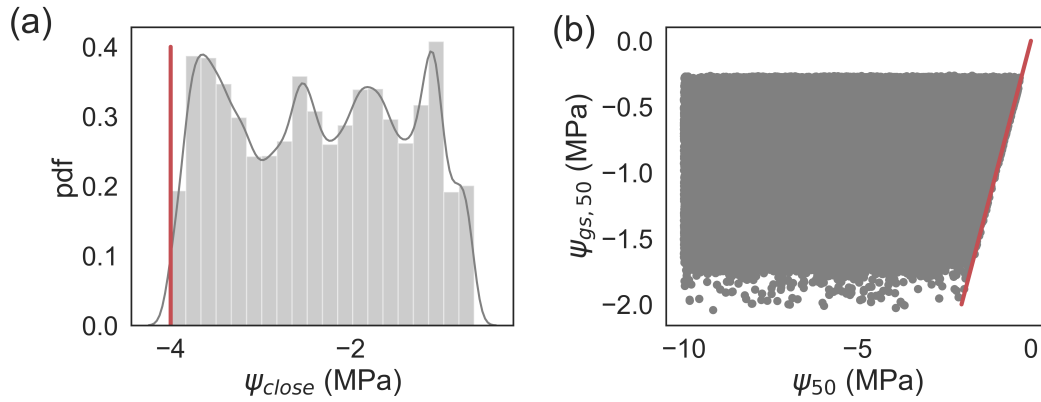Figure 1: Physiological constraints imposed in MCMC. (a) Distribution of leaf water potential (daily average) at full stomatal closure (ψ_{close}) across the studied sites and MCMC samples for each site (grey area). (b) Scatter of the leaf water potential (daily average) at half stomatal closure ($\psi_{gs,50}$) and ψ_{50} across the studied sites and MCMC samples for each site. The red lines denote the constraints based on meta-analysis [3, 4].
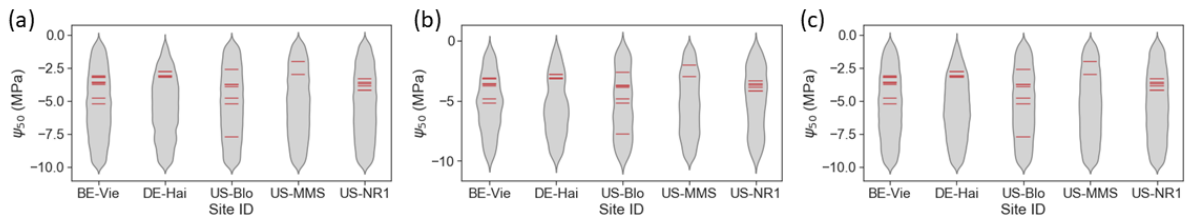
Figure 2: Posterior distributions of ψ_{50} at five example sites estimated with (a) 20% shallower, (b) the same, and (c) 20% deeper roots as listed in Table S1. Refer to Fig. 1 (main text) for detailed description of symbols.
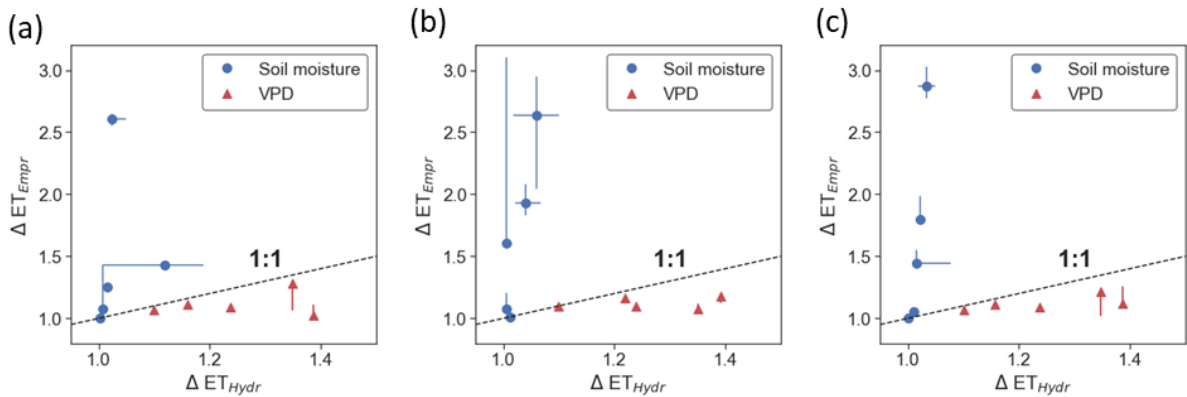

Figure 3: The restriction effect of soil moisture and VPD on ET at five example sites (Supplementary Fig. 2) based on the hydraulic and empirical models estimated with (a) 20% shallower, (b) the same, and (c) 20% deeper roots as listed in Table S1. Refer to Fig. 3 (main text) for detailed description on symbols.

Supplementary References

[1] Campbell, G. S. & Norman, J. M. *An introduction to environmental biophysics* (Springer-Verlag, New York, 1998).

[2] Bonan, G. B. Land surface model (LSM version 1.0) for ecological, hydrological, and atmospheric studies: Technical description and users guide. Technical note. Tech. Rep., National Center for Atmospheric Research, Boulder, CO, United States (1996).

[3] Martin-StPaul, N., Delzon, S. & Cochard, H. Plant resistance to drought depends on timely stomatal closure. *Ecology Letters* **20**, 1437–1447 (2017).

[4] Anderegg, W. R. *et al.* Plant water potential improves prediction of empirical stomatal models. *PloS One* **12**, e0185481 (2017).

[5] Bartlett, M. K., Klein, T., Jansen, S., Choat, B. & Sack, L. The correlations and sequence of plant stomatal, hydraulic, and wilting responses to drought. *Proceedings of the National Academy of Sciences* **113**, 13098–13103 (2016).

[6] Mencuccini, M., Minunno, F., Salmon, Y., Martínez-Vilalta, J. & Hölttä, T. Coordination of physiological traits involved in drought-induced mortality of woody plants. *New Phytologist* **208**, 396–409 (2015).

[7] Kilinc, M., Beringer, J., Hutley, L. B., Tapper, N. J. & McGuire, D. A. Carbon and water exchange of the world's tallest angiosperm forest. *Agricultural and forest meteorology* **182**, 215–224 (2013).

[8] Moureaux, C., Debacq, A., Bodson, B., Heinesch, B. & Aubinet, M. Annual net ecosystem carbon exchange by a sugar beet crop. *Agricultural and Forest Meteorology* **139**, 25–39 (2006).

[9] Aubinet, M. *et al.* Long term carbon dioxide exchange above a mixed forest in the Belgian Ardennes. *Agricultural and Forest Meteorology* **108**, 293–315 (2001).

[10] Mkhabela, M. *et al.* Comparison of carbon dynamics and water use efficiency following fire and harvesting in Canadian boreal forests. *Agricultural and Forest Meteorology* **149**, 783–794 (2009).

[11] Dietiker, D., Buchmann, N. & Eugster, W. Testing the ability of the DNDC model to predict CO2 and water vapour fluxes of a Swiss cropland site. *Agriculture, ecosystems & environment* **139**, 396–401 (2010).

[12] Guan, D.-X. *et al.* CO_2 fluxes over an old, temperate mixed forest in northeastern China. *Agricultural and Forest Meteorology* **137**, 138–149 (2006).

[13] Anthoni, P. *et al.* Forest and agricultural land-use-dependent CO2 exchange in Thuringia, Germany. *Global Change Biology* **10**, 2005–2019 (2004).

[14] Knohl, A., Schulze, E.-D., Kolle, O. & Buchmann, N. Large carbon uptake by an unmanaged 250-year-old deciduous forest in Central Germany. *Agricultural and Forest Meteorology* **118**, 151–167 (2003).

[15] Prescher, A.-K., Grünwald, T. & Bernhofer, C. Land use regulates carbon budgets in eastern Germany: From NEE to NBP. *Agricultural and Forest Meteorology* **150**, 1016–1025 (2010).

[16] Lindauer, M. *et al.* Net ecosystem exchange over a non-cleared wind-throw-disturbed upland spruce forest—Measurements and simulations. *Agricultural and forest meteorology* **197**, 219–234 (2014).

[17] Schmidt, M., Reichenau, T. G., Fiener, P. & Schneider, K. The carbon budget of a winter wheat field: An eddy covariance analysis of seasonal and inter-annual variability. *Agricultural and Forest Meteorology* **165**, 114–126 (2012).

[18] Pilegaard, K., Ibrom, A., Courtney, M. S., Hummelshøj, P. & Jensen, N. O. Increasing net CO_2 uptake by a Danish beech forest during the period from 1996 to 2009. *Agricultural and Forest Meteorology* **151**, 934–946 (2011).

[19] Bäck, J. *et al.* Chemodiversity of a Scots pine stand and implications for terpene air concentrations. *Biogeosciences* **9**, 689–702 (2012).

[20] Loubet, B. *et al.* Carbon, nitrogen and Greenhouse gases budgets over a four years crop rotation in northern France. *Plant and Soil* **343**, 109 (2011).

[21] Berbigier, P., Bonnefond, J.-M. & Mellmann, P. CO_2 and water vapour fluxes for 2 years above Euroflux forest site. *Agricultural and Forest Meteorology* **108**, 183–197 (2001).

[22] Sabbatini, S. *et al.* Greenhouse gas balance of cropland conversion to bioenergy poplar short-rotation coppice. *Biogeosciences* **13**, 95–113 (2016).

[23] Valentini, R. *et al.* Seasonal net carbon dioxide exchange of a beech forest with the atmosphere. *Global Change Biology* **2**, 199–207 (1996).

[24] Ferréa, C., Zenone, T., Comolli, R. & Seufert, G. Estimating heterotrophic and autotrophic soil respiration in a semi-natural forest of Lombardy, Italy. *Pedobiologia* **55**, 285–294 (2012).

[25] Marcolla, B., Pitacco, A. & Cescatti, A. Canopy architecture and turbulence structure in a coniferous forest. *Boundary-layer meteorology* **108**, 39–59 (2003).

[26] Marcolla, B. *et al.* Climatic controls and ecosystem responses drive the inter-annual variability of the net ecosystem exchange of an alpine meadow. *Agricultural and forest meteorology* **151**, 1233–1243 (2011).

[27] Migliavacca, M. *et al.* Modeling gross primary production of agro-forestry ecosystems by assimilation of satellite-derived information in a process-based model. *Sensors* **9**, 922–942 (2009).

[28] Montagnani, L. *et al.* A new mass conservation approach to the study of CO_2 advection in an alpine forest. *Journal of Geophysical Research: Atmospheres* **114** (2009).

[29] Rey, A. *et al.* Annual variation in soil respiration and its components in a coppice oak forest in Central Italy. *Global Change Biology* **8**, 851–866 (2002).

[30] Jacobs, C. M. J. *et al.* Variability of annual CO_2 exchange from dutch grasslands. *Biogeosciences* **4**, 803–816 (2007). URL https://www.biogeosciences.net/4/803/2007/.

[31] Kurbatova, J., Li, C., Varlagin, A., Xiao, X. & Vygodskaya, N. Modeling carbon dynamics in two adjacent spruce forests with different soil conditions in Russia. *Biogeosciences* **5**, 969–980 (2008).

[32] Fares, S. *et al.* Tropospheric ozone reduces carbon assimilation in trees: estimates from analysis of continuous flux measurements. *Global Change Biology* **19**, 2427–2443 (2013).

[33] Law, B., Thornton, P., Irvine, J., Anthoni, P. & Van Tuyl, S. Carbon storage and fluxes in ponderosa pine forests at different developmental stages. *Global Change Biology* **7**, 755–777 (2001).

[34] Brzostek, E. R. *et al.* Chronic water stress reduces tree growth and the carbon sink of deciduous hardwood forests. *Global change biology* **20**, 2531–2539 (2014).

[35] Burns, S. P. *et al.* A comparison of the diel cycle of modeled and measured latent heat flux during the warm season in a Colorado subalpine forest. *Journal of Advances in Modeling Earth Systems* **10**, 617–651 (2018).

[36] Matheny, A. M. *et al.* Species-specific transpiration responses to intermediate disturbance in a northern hardwood forest. *Journal of Geophysical Research: Biogeosciences* **119**, 2292–2311 (2014).

[37] Nave, L. *et al.* Disturbance and the resilience of coupled carbon and nitrogen cycling in a north temperate forest. *Journal of Geophysical Research: Biogeosciences* **116** (2011).